Anderson localization of excitations in disordered Gross-Pitaevskii lattices

Yagmur Kati [1,2,*] Mikhail V. Fistul [1,3,4,†] Alexander Yu. Cherny [1,5,‡] and Sergej Flach[1,2,§]

[1]*Center for Theoretical Physics of Complex Systems, Institute for Basic Science, Daejeon 34051, Korea*
[2]*Basic Science Program, Korea University of Science and Technology (UST), Daejeon 34113, Republic of Korea*
[3]*Theoretische Physik III, Ruhr-University Bochum, Bochum 44801, Germany*
[4]*National University of Science and Technology "MISIS", Moscow 119049, Russia*
[5]*Bogoliubov Laboratory of Theoretical Physics, Joint Institute for Nuclear Research, Dubna 141980, Moscow region, Russia*

We examine the one-dimensional Gross-Pitaevskii lattice at zero temperature in the presence of uncorrelated disorder. We obtain analytical expressions for the thermodynamic properties of the ground state field and compare them with numerical simulations both in the low- and high-density regimes. We analyze weak excitations above the ground state and compute the localization properties of Bogoliubov–de Gennes modes. In the long-wavelength limit, these modes delocalize in accordance with the extended nature of the ground state. For high densities, we observe and derive a divergence of their localization length at finite energy due to an effective correlated disorder induced by the weak ground state field fluctuations. We derive effective high-density field equations for the excitations and generalize to higher dimensions.

I. INTRODUCTION

Trapped ultracold atoms have been used for many years as an ideal playground to study the properties of a variety of model classes of interacting bosons in the presence of external potentials [1–5]. Periodic optical potentials, obtained with the counterpropagating laser beams [6], allow for emulating the physics of interacting particles in almost arbitrarily tunable crystal fields. Artificially created random potentials enable the direct observation of Anderson localization [7–9]. Such systems allow for the observation of Bose-Einstein condensation of ultracold atoms. The dynamics of the Bose-Einstein condensate is successfully described by the Gross-Pitaevskii (GP) model [10,11].

The thermodynamic properties of the GP lattice model [12,13] are determined by two conserved quantities [12,14]: the particle density a and the energy density h. The two relevant energy scales are the interaction energy ga (here g is the interaction induced nonlinearity strength g) and the kinetic energy J due to the tunneling between adjacent lattice sites. In Ref. [12] the complete phase diagram h-a has been obtained for a one-dimensional (1D) GP chain in the absence of disorder. Various peculiar effects, e.g., a dynamical glass behavior [14], non-Gibbsian phases [12], and long-lived spatially localized rare fluctuations forming at high temperatures [15], have been predicted and observed in extensive simulations.

An ordered GP model has a spatially homogeneous ground state. Weak excitations above that ground state result in spa-

tially extended Bogoliubov–de Gennes modes [16]. Their properties have been studied for spatially continuous systems using the Bogoliubov–de Gennes (BdG) theory [16–19]. The spectrum of these excitations was verified in experiments with atomic Bose-Einstein condensates (see the reviews [3,4]). The interplay of nonlinearity, discreteness of the media, interaction, and spatial disorder results in novel phenomena. Disorder introduces an additional energy scale W. It induces long-time relaxation dynamics and glass phases, the Anderson localization [20], and the Lifshits glass phase [21–25], to name a few. The presence of interactions strongly influences Anderson localization (see, e.g., the reviews [26–28]). For bosons, repulsive interactions tend to delocalize excitations [26]. A number of previous studies have analyzed the long-wavelength properties of BdG excitations in one-dimensional disordered GP models [29–37] in order to address superfluidity and various phase transitions.

In this work, we address the properties of the one-dimensional disordered GP lattice by going beyond the long-wavelength limit. We compute the ground state dependence $h(a)$ both in the low-density ($ga \ll J, W$) and the high-density ($ga \gg J, W$) regimes. The low-density ground state is characterized by rare regions with nonzero particle density separated by large empty parts due to the Lifshits tail states. The high-density ground state is almost homogeneous with weak fluctuations induced by the disorder field. We compute the ground state using efficient numerical schemes and find quantitative agreement with analytical approximations. We then proceed with computing the localization properties (localization length ξ and participation number P) of BdG excitations. Exact numerical diagonalization confirms the divergence of ξ and P in the long-wavelength limit. This is due to the fact that the BdG zero-energy eigenmode becomes a copy of the ground state in that limit. We then report on

*ygmrkati@gmail.com
†Mikhail.Fistul@ruhr-uni-bochum.de
‡alexander.yu.cherny@gmail.com
§sflach@ibs.re.kr

a surprising anomalous enhancement of ξ and P of BdG modes at finite energy in the high-density regime. We aim at an analytical description by performing a systematic perturbation approach using first the exact BdG equations and an approximate ground state field. We then proceed with approximating the equations as well and obtain the disordered BdG equations in the leading order for the high-density regime. These equations reduce the eigenvalue problem to a one-dimensional chain with short-range correlated disorder, for which the localization length can be computed analytically. We find full agreement of our results between all stages of approximations. Most importantly, the analytical solution yields a full divergence of the localization length at finite energy. We conclude with a discussion of possible generalizations to higher-dimensional lattice cases.

While our analysis is motivated by its direct application to the Bose-Einstein condensation in systems of ultracold atoms, it can also provide useful insight into the thermodynamic and dynamic properties of the Bose-glass phase and the Bose-glass–superfluid quantum phase transition [38–44] obtained in strongly disordered or granular two-dimensional superconductors [45,46] and vortex lattices in layered superconductors [47].

The paper is organized as follows. In Sec. II we introduce the model. In Sec. III we study the ground state properties by combining the analytical and numerical approaches. In Sec. IV we compute the localization properties of the BdG excitations. We conclude with Sec. V.

II. MODEL

We consider a disordered Gross-Pitaevskii (GP) model on a one-dimensional lattice. The model describes, e.g., the properties of a Bose-Einstein condensate of ultracold atoms loaded onto an optical lattice formed by counterpropagating laser beams. The dynamics of such a system is governed by the Hamiltonian

$$\mathcal{H} = \sum_{\ell=1}^{N} \frac{g}{2} |\psi_\ell|^4 + \epsilon_\ell |\psi_\ell|^2 - J(\psi_\ell \psi_{\ell+1}^* + \psi_\ell^* \psi_{\ell+1}). \quad (1)$$

ψ_ℓ is the condensate wave-function amplitude on lattice site $1 \leqslant \ell \leqslant N$. The nonlinearity parameter g is related to the strength of two-body interactions in the condensate on the same site, and J is the hopping strength between neighboring sites, which is related to the tunneling rate of a single particle. The on-site energies ϵ_ℓ describe the spatial disorder imprinted into the system, and take random uncorrelated values with a probability distribution function $\rho(\epsilon)$ being constant in the region $[-W/2, W/2]$ and zero outside. Hence, its mean value and variance are given by $\langle \epsilon_\ell \rangle = 0$ and $\langle \epsilon_\ell^2 \rangle = W^2/12$, respectively.

The Hamiltonian equations of motion $\dot{\psi}_\ell = \partial \mathcal{H}/\partial (i\psi_\ell^*)$ result in

$$i\dot{\psi}_\ell = \epsilon_\ell \psi_\ell + g|\psi_\ell|^2 \psi_\ell - J(\psi_{\ell+1} + \psi_{\ell-1}). \quad (2)$$

The discrete GP equation possesses two integrals of motion: the total energy $\mathcal{H}$ and norm $\mathcal{A} = \sum_\ell |\psi_\ell|^2$. The energy can be measured in units of J, and the uniform rescaling of the average norm $a = \mathcal{A}/N$ tunes the nonlinearity g. Therefore we

fix $J = 1$ and $g = 1$ for the numerical computations to come, but keep them explicitly in all analytical expressions.

III. GROUND STATE PROPERTIES

The dynamics of the system depends on the two energy and norm densities $h = \mathcal{H}/N$ and $a = \mathcal{A}/N$. For a fixed value of a, the GP model has a ground state (GS) of minimum energy, which is characterized by the lowest possible value of h. The ground state can be obtained using the method of Lagrange multipliers:

$$\mathcal{L} = \mathcal{H} - \mu \mathcal{A}, \quad \frac{\partial \mathcal{L}}{\partial \psi_\ell^*} = \frac{\partial \mathcal{L}}{\partial \psi_\ell} = 0. \quad (3)$$

It follows from Eqs. (1) and (3)

$$\mu \psi_\ell = \epsilon_\ell \psi_\ell + g|\psi_\ell|^2 \psi_\ell - J(\psi_{\ell+1} + \psi_{\ell-1}), \quad (4)$$

where μ is the chemical potential (Lagrangian multiplier). Comparing Eqs. (2) and (4) yields

$$\psi_\ell(t) = G_\ell e^{-i\mu t}, \quad (5)$$

where $G_\ell = \psi_\ell(0) \geqslant 0$ can be chosen to be real and non-negative. We then obtain the set of equations that determines the ground state amplitude field G_ℓ

$$G_\ell^2 = (\mu - \epsilon_\ell + J\zeta_\ell)/g, \quad \zeta_\ell = (G_{\ell+1} + G_{\ell-1})/G_\ell \quad (6)$$

with the ground state correlation field ζ_ℓ.

We note that the ground state solution for the ordered case $W = 0$ is simply $G_\ell^2 = a$. Using Eq. (1) we arrive at the analytical dependence $h = ga^2/2 - 2aJ$, which is shown as a dotted black line in Fig. 1(a).

In the presence of disorder, there are three competing energy density scales: the kinetic J, disorder W, and interaction ga energy densities, respectively. For all studied cases we use $W = 4$. We distinguish the regime of low-density $ga \ll W$ and high-density $ga \gg W$. By fixing the norm density, we numerically minimize the energy by varying the real and non-negative variables G_ℓ for a given disorder realization as in Ref. [24] (see also Appendix A). The resulting ground state density distribution G_ℓ^2 is plotted in Fig. 1 for two different norm densities: $a = 0.01$ and $a = 5$, with one and the same disorder realization. For each outcome, we compute the total energy and the corresponding energy density. We then toss a new disorder realization and repeat the process N_r times. We finally compute the average energy density h and its standard deviation. The resulting dependence $h(a)$ is shown with red circles in Fig. 1(a), where the error bars are the standard deviation. We find that for nonzero W (here $W = 4$) the curve $h(a)$ shifts to lower energies as compared to the ordered $W = 0$ curve.

Averaging both sides of Eq. (6) over all sites in an infinite system yields the chemical potential

$$\mu = ga - J\bar{\zeta}, \quad (7)$$

with the average GS correlation field value $\bar{\zeta} = \langle \zeta_\ell \rangle$. Inserting Eq. (7) into Eq. (6) leads to

$$gG_\ell^2 = ga - \epsilon_\ell + J\delta\zeta_\ell \geqslant 0, \quad (8)$$

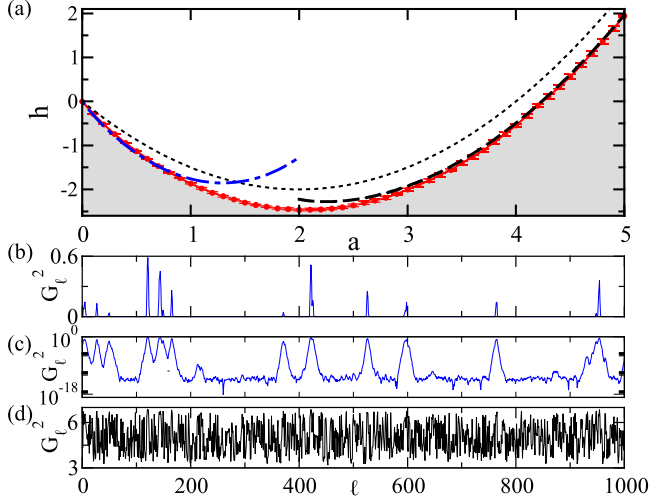where $\delta\zeta_\ell = \zeta_\ell - \bar{\zeta}$ describes the fluctuations of the GS correlation field.

FIG. 1. (a) The ground state energy density h versus norm density a. Red circles connected with lines are the results of the numerical calculation for $W = 4$, $N = 10000$, $N_r = 50$, and the error bars are the corresponding standard deviations due to disorder realization averaging. The dotted black line corresponds to the ordered case $W = 0$. Dashed-dotted blue line: low-density approximation Eq. (16). Dashed black line: high-density approximation Eq. (19). (b) G_ℓ^2 versus l for one disorder realization with $a = 0.01$ and $W = 4$. (c) Same as (b) but with G_ℓ^2 on logarithmic scale to highlight exponential localization and non-negativity. (d) G_ℓ^2 versus ℓ for one disorder realization with $a = 5$, and $W = 4$. Note that $g = 1$, $J = 1$ for all cases.

The inhomogeneity of the ground state is measured with its participation number density

$$p = \frac{Na^2}{\sum_\ell^N |G_\ell|^4}, \quad 0 \leqslant p \leqslant 1. \tag{9}$$

For $p \to 1$ the GS turns homogeneous, while $p \to 0$ indicates a sparse GS. We varied the system size from $N = 1000$ to $N = 10000$ to check and observe that p does not vary with N. The independence of p on N provides evidence for the delocalized GS and also excludes impact of multifractality effects obtained in high-dimensional systems [48]. The numerical evaluation of $p(a)$ is shown in Fig. 2. We find that p takes small values in the low-density regime as seen also by a GS realization in Fig. 1(b). In the high-density regime, p tends to one, thus indicating a more and more homogeneous GS distribution as seen also by a GS realization in Fig. 1(c). The inset in Fig. 2 shows the computed $\mu(a)$ dependence. In particular, $\mu(a \to 0) \to -2J - W/2 = -4$, while $\mu = ga - 2J$ in the high-density regime.

The GS correlation field ζ_l characteristics are captured by its average $\bar{\zeta}$ and standard deviation σ_ζ. Their dependence on a is represented in Fig. 3. In the high-density regime, it quickly approaches its asymptotic value $\bar{\zeta} = 2$. The standard deviation $\sigma_\zeta \sim 1/a$ tends to zero in the same high-density limit (see also inset in Fig. 3). The same inset also shows that the covariance $\mathrm{cov}(\epsilon, \zeta) = \langle \epsilon_\ell \delta \zeta_\ell \rangle$ is tending to zero in a similar way in the high-density regime. However, the relative correlation $r(\epsilon, \zeta) = \mathrm{cov}(\epsilon, \zeta)/\sigma_\epsilon \sigma_\zeta \approx 0.8$ appears to be almost constant and nonzero in the limit of high densities,
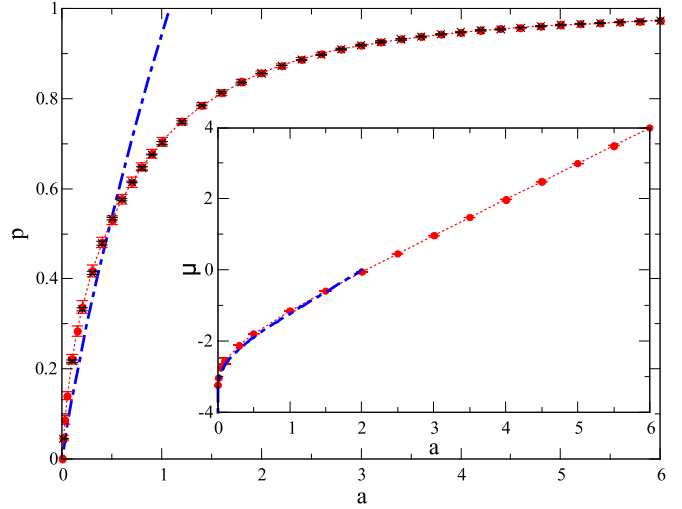

FIG. 2. The ground state participation number density p versus the particle density a for $N = 1000$ (red circles) and $N = 10000$ (black crosses). Error bars represent the standard deviation of the data. Dotted lines connect the data and guide the eye. The blue dashed-dotted line is obtained from Eq. (14). Inset: The chemical potential μ versus a (red circles). Error bars represent the standard deviations of the data. Dotted lines connect the data and guide the eye. The blue dashed-dotted line is obtained from Eq. (13). $N = 1000$, $N_r = 100$, $W = 4$, $g = 1$, $J = 1$ for both plots.

indicating that whatever weak the GS correlation field fluctuations may become, they still carry some nontrivial correlations with the disorder field.

A. Low-density regime

In the low particle density regime, i.e., as $ga \ll W$ the ground state G_ℓ is a strongly inhomogeneous one. In order
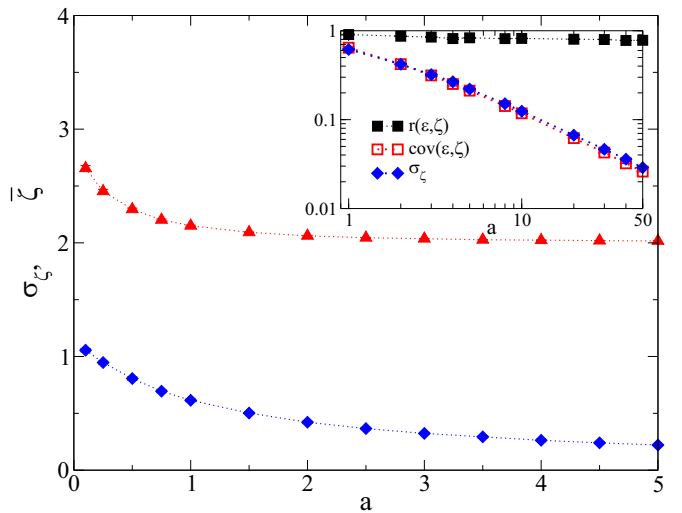

FIG. 3. The average GS correlation field value $\bar{\zeta}$ (red filled triangles) and its variance σ_ζ (blue filled diamonds) vs a. Inset: σ_ζ (blue filled diamonds), $\mathrm{cov}(\epsilon, \zeta)$ (red open squares) and $r(\epsilon, \zeta)$ (black filled squares) versus a on logarithmic scales. $N = 1000$, $N_r = 100$, $W = 4$, $g = 1$, $J = 1$ for both plots. Connecting dotted lines guide the eye.

to satisfy Eq. (6), it has to be contained by a large amount of well-separated particle clusters of size $L \geqslant 1$ [see Fig. 1(b)]. The particles concentrate in the deepest minima of the on-site energy landscape, and the number of particles outside the clusters is exponentially small. Let us perform a quantitative analysis of these so-called Lifshits states [21]. Let ρ_1 be the probability of finding a particle on site ℓ. The on-site energy ϵ_ℓ has to satisfy the condition $\epsilon_\ell < \mu + J\zeta_\ell$. We use the probability $\rho_c(\mu)$ to obtain particles in a connected cluster of size L [49]

$$\rho_c(\mu) = \rho_1{}^L = \left[\int_{-W/2}^{\mu+2J} \rho \, d\epsilon \right]^L = \left[\frac{\mu + 2J + W/2}{W} \right]^L. \quad (10)$$

The cluster size L is obtained as follows. Inside a cluster, the ground state G_ℓ satisfies the linearized Eq. (4) with minimal on-site energy, $\epsilon_\ell = -W/2$. Therefore, $G_\ell \simeq \sin(q_0\ell)$, where q_0 is determined as $q_0 = \sqrt{(\mu + 2J + W/2)/J}$. Taking into account that $G_\ell \simeq 0$ outside the cluster, we obtain the explicit expression

$$L(\mu) = \pi \sqrt{\frac{J}{\mu + 2J + W/2}}. \quad (11)$$

The total norm can be approximated as the product of the total number of clusters N_0, multiplied by their amplitudes A_0, and the cluster size L:

$$\mathcal{A} = \sum_\ell \psi_\ell{}^2 = N_0 A_0 L = N\rho_c(\mu)A_0 L. \quad (12)$$

Using Eq. (12) it follows

$$ga = gA_0 L \rho_c(\mu) \approx 2 \left[\frac{\mu + 2J + W/2}{W} \right]^L, \quad (13)$$

where $gA_0 L \approx 2$, as found numerically. Substituting (11) in (13) and solving the resulting transcendent equation we obtain the dependence of the chemical potential on the norm density $\mu(a)$. This dependence is plotted in the inset of Fig. 2 by the dashed-dotted line and shows very good agreement with the numerically computed $\mu(a)$ dependence.

Similarly, we obtain the dependence of the ground state participation number density p on the chemical potential μ as

$$p = \frac{\left(\sum_\ell \psi_\ell{}^2 \right)^2}{\sum_\ell \psi_\ell{}^4} = \frac{(A_0 L \rho_c(\mu)N)^2}{A_0{}^2 L \rho_c(\mu)N} = N\rho_c(\mu)L. \quad (14)$$

With Eq. (13) it follows

$$p = N\frac{L}{2}ga. \quad (15)$$

Using (11) and (13) we obtain the $p(a)$ dependence plotted in Fig. 2, which shows good agreement with the numerically computed result.

Finally, we can compute the ground state energy density by substituting (14) into the exact relation $h = \mu a - Nga^2/2p$:

$$h = \mu a - \frac{ga^2}{2\rho_c(\mu)L} = \left(\mu - \frac{1}{L} \right)a. \quad (16)$$

This dependence is plotted in Fig. 1 by the dashed-dotted blue line and shows very good agreement with the numerical result for small values of $a < 1$.

B. High-density regime

In the high-density regime, we have $\max\{W, J\} \ll ga$. First, we use Eq. (8) when $J/(ga) \ll 1$

$$G_\ell \simeq \sqrt{a - \frac{\epsilon_l}{g}}. \quad (17)$$

This local density approximation of the ground state works better for higher densities because the condensate healing length becomes shorter and shorter. Using Eqs. (1) and (5) and averaging over all sites with respect to disorder yield

$$h = \langle \epsilon_\ell G_\ell{}^2 \rangle + \frac{g}{2}\langle G_\ell{}^4 \rangle - 2J\langle G_\ell G_{\ell+1} \rangle. \quad (18)$$

This finally leads to the energy density of the ground state in the high-density regime (see also Appendix B)

$$h \approx \frac{g}{2}\left(a^2 - \frac{w^2}{12} \right) - \frac{8J}{9w^2}\left[\left(a + \frac{w}{2} \right)^{3/2} - \left(a - \frac{w}{2} \right)^{3/2} \right]^2, \quad (19)$$

where we denote $w = W/g$. The corresponding black dashed curve for $W = 4$ in Fig. 1 shows very good agreement with the numerically computed ground state line $h(a)$ in the high-density regime.

Note that in the high-density regime we can further expand Eq. (17) in small parameter $W/(ga)$

$$G_\ell \simeq \sqrt{a}\left[1 - \frac{\epsilon_l}{2ga} \right]. \quad (20)$$

Then the resulting ground state energy is very close to that of Eq. (19).

IV. ELEMENTARY EXCITATIONS

We consider weak (small amplitude) excitations above the ground state by introducing a small perturbation to the ground state G_ℓ:

$$\psi_\ell(t) = [G_\ell + \delta_\ell(t)]e^{-i\mu t}. \quad (21)$$

Linearizing the equations of motion (2) with respect to δ, we arrive at

$$i\dot{\delta}_\ell = (\epsilon_\ell - \mu)\delta_\ell + gG_\ell{}^2(\delta_\ell^* + 2\delta_\ell) - J(\delta_{\ell+1} + \delta_{\ell-1}). \quad (22)$$

With the choice

$$\delta_\ell(t) = \chi_\ell e^{-i\lambda t} - \Pi_\ell^* e^{i\lambda t} \quad (23)$$

and the use of Eq. (6) we obtain the BdG eigenvalue equations for the two interacting excitation fields χ and Π as

$$\lambda\chi_\ell = J\zeta_\ell\chi_\ell - J(\chi_{\ell+1} + \chi_{\ell-1}) - gG_\ell{}^2(\Pi_\ell - \chi_\ell),$$

$$\lambda\Pi_\ell = -J\zeta_\ell\Pi_\ell + J(\Pi_{\ell+1} + \Pi_{\ell-1}) + gG_\ell{}^2(\chi_\ell - \Pi_\ell). \quad (24)$$

We stress that the right-hand side (RHS) of the above BdG equations contains only the GS field G_l as input. The BdG equations are particle-hole symmetric $[\lambda_\nu, \{\chi_\ell{}^\nu, \Pi_\ell{}^\nu\}] \longleftrightarrow [-\lambda_\nu, \{\Pi_\ell{}^\nu, \chi_\ell{}^\nu\}]$ (ν is the mode number). This yields the solution $\chi_\ell = \Pi_\ell \propto G_l$ for $\lambda_\nu = 0$ as follows also readily from inspecting (24), independently of the choice of the GS field. The eigenvector to $\lambda = 0$ can be also obtained from the observation that δ_ℓ is time independent by Eq. (23). Then it follows from Eq. (21) that δ_ℓ is proportional to G_ℓ. Due to this

proportionality, the BdG eigenvector to $\lambda = 0$ is delocalized in space, just as G_ℓ is for any finite norm density a (see also Ref. [19]).

Next we use the decomposition $\chi_\ell = (S_\ell + D_\ell)/2$ and $\Pi_\ell = (S_\ell - D_\ell)/2$ we arrive at the (still) exact set of equations

$$\lambda S_\ell = (J\zeta_\ell + 2gG_\ell^2)D_\ell - J(D_{\ell+1} + D_{\ell-1}), \quad (25)$$

$$\lambda D_\ell = J\zeta_\ell S_\ell - J(S_{\ell+1} + S_{\ell-1}). \quad (26)$$

Inserting (26) into (25) yields

$$\frac{\lambda^2}{J}S_\ell = (J\zeta_\ell + 2gG_\ell^2)(\zeta_\ell S_\ell - S_{\ell+1} - S_{\ell-1})$$
$$- J(\zeta_{\ell+1}S_{\ell+1} + \zeta_{\ell-1}S_{\ell-1} - S_{\ell-2} - 2S_\ell - S_{\ell+2}). \quad (27)$$

BdG modes to nonzero values of λ are expected to be Anderson localized due to the presence of disorder and the one-dimensionality of the system.

A. Numerical results

We numerically calculate the participation number of each mode as

$$P_\nu = \frac{\left(\sum_\ell^N n_{\ell,\nu}\right)^2}{\sum_\ell^N n_{\ell,\nu}^2}, \quad n_{\ell,\nu} = |\chi_{\ell,\nu}|^2 + |\Pi_{\ell,\nu}|^2, \quad (28)$$

where $\nu = 1, \ldots, 2N$ is the mode number. We divide the λ axis into small bins of size 0.05, and average the participation numbers in each bin to obtain the dependence $\bar{P}(\lambda)$. The system size is $N = 10^5$, and we used three disorder realizations (except for $a = 10$ with only one disorder realization). For smaller system size $N = 10^4$ we increased the number of realizations, with results matching the plotted results very well (not shown here). Essentially there is a tradeoff due to the computational limitations on the CPU time. In addition there is a limitation in the computation of large systems, which comes from both the ground state computation, and the diagonalization of large matrices for the BdG modes. Since we intend to compute large participation numbers, we choose the largest possible system sizes. The fact that the number of realization is small does not impact the statistical fidelity of the curves, since the λ axis is binned with a fixed bin size, and larger system sizes lead to more data per bin and thus to more statistical reliability.

The resulting curves are plotted in Fig. 4 for different norm densities and $W = 4$. We observe symmetric curves $\bar{P}(\lambda) = \bar{P}(-\lambda)$ due to the above-mentioned particle-hole symmetry of the BdG eigenvalue problem. All curves show a clear divergence $\bar{P}(|\lambda| \to 0) \to \infty$, which is only limited due to finite-size effects. This divergence agrees with the above result that the BdG mode at zero energy $\lambda = 0$ must be delocalized and thus have an infinite participation number. The divergence has been addressed in a number of publications [19,25,29–32], which results in $\bar{P} \sim 1/|\lambda|^\alpha$ with $\alpha = 2$ in the high-density regime [30,32,50].

The participation numbers at nonzero energies show an expected finite height peak in the low-density regime, which is a peak continuation from the zero interaction limit (Fig. 4).
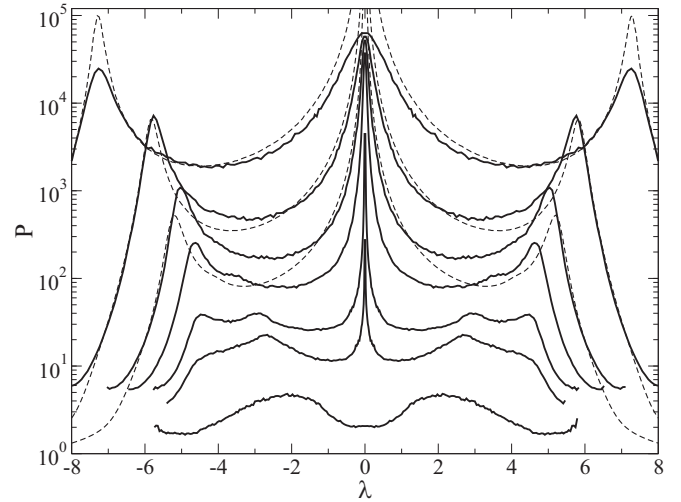

FIG. 4. The bin average participation number $\bar{P}$ of BdG modes versus the energy λ. Solid lines - numerical computation with $N = 10^5$, $W = 4$ and $a = 0, 0.5, 1, 2, 3, 5, 10$ from bottom to top, and $N_r = 3$. Thick dashed lines: transfer matrix calculation results of the localization length $1.5 \times \xi(\lambda)$ for $a = 3, 5, 10$ with 10^8 iterations of (27) (see text for details). Note that all localization length data are multiplied with one and the same scaling factor 1.5.

In that limit, the BdG eigenvalue equations decompose into two copies of the tight-binding chain with on-site disorder. The largest localization length and participation number are then obtained in the centers of their spectra $\lambda = \pm\mu$, which host the largest density of states [49]. Upon crossing over from the low-density to the high-density regime, we observe a second peak developing at larger absolute λ values, which has a finite height, but which appears to grow swiftly (Fig. 4). This new side peak results in an unexpected enhancement of the participation number, localization length, and size of BdG modes at finite energies λ in the high-density regime.

B. Finite energy localization length singularity for high densities

In order to analytically assess the observed side peak of the BdG modes in the high-density regime $ga \gg W$, we use the exact equations (27) with the approximated GS field (20) and compute the localization length $\xi(\lambda)$ with a transfer matrix method (see Appendix C). The resulting curves are plotted in Fig. 4 for $a = 3, 4, 5, 10$ and show almost full quantitative agreement with the numerical results from the exact equations and the numerically exact GS for $a = 10$, while the agreement is less quantitative but still qualitative as the value of a is reduced. Therefore we can use the approximate GS field (20) with the exact equations (27) as a reliable reference for even larger values of $a > 10$, which are not accessible by brute force numerical computations due to system size limitations and the increase of the participation number and localization length with further density increase. The resulting dependence $\xi(\lambda)$ is shown in Fig. 5 for $a = 100$. The side peak is not only remaining in place but is also increasing its height relative to the background.

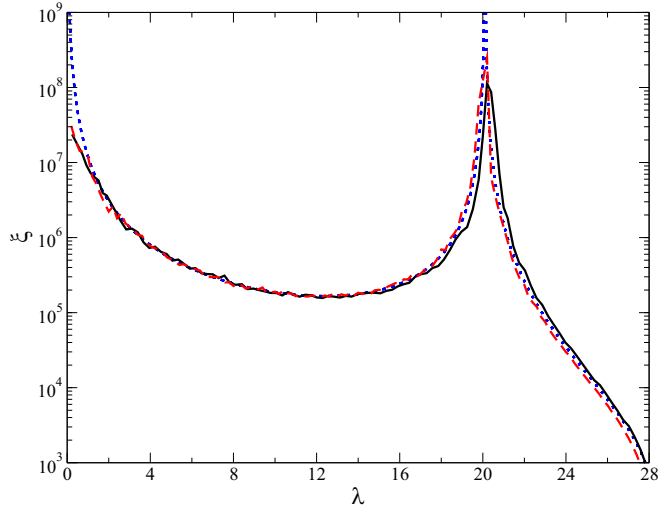In the high-density limit, $ga \gg W$, deeper insight on the localization properties of BdG modes can be obtained. We

FIG. 5. The localization length $\xi(\lambda)$ for $a = 100$, $g = J = 1$, $W = 4$. Black solid line: exact BdG equations (27), approximate GS field (20), transfer matrix calculation results with 10^8 iterations. Red thick dashed line: approximate BdG equations (29), approximate GS field (20), transfer matrix calculation results with 10^8 iterations. Blue thick dotted line: analytical result (32) with (D7).

simplify the exact Eq. (27) keeping only the leading-order term on the RHS of (27), and arrive at

$$\frac{\lambda^2}{J}S_\ell = 2gG_\ell^2(\zeta_\ell S_\ell - S_{\ell-1} - S_{\ell+1}). \quad (29)$$

Note that $\lambda = 0$ and $S_l = G_l$ is still a valid solution. We again compute the localization length $\xi(\lambda)$ using (29) and the GS field approximation (20). The resulting curve for $a = 100$ agrees quantitatively with the exact equation result in Fig. 5, confirming the validity of our equation approximation.

Defining the dimensionless energy E as $E = \lambda^2/(2gaJ)$ we cast Eq. (29) into the standard form

$$(\tilde{E} + \varkappa_\ell)S_\ell = S_{\ell-1} + S_{\ell+1} \quad (30)$$

with

$$\tilde{E} = \langle \zeta_\ell \rangle - E\langle a/G_\ell^2 \rangle, \quad \varkappa_\ell = \zeta_\ell - E\frac{a}{G_\ell^2} - \tilde{E}. \quad (31)$$

In the high-density regime $ga \gg W$, $\tilde{E} = 2 - E$ and the perturbing random potential $\varkappa_\ell$ is small, with its expectation value being zero: $\langle \varkappa_\ell \rangle = 0$. The disorder field ϵ_ℓ is uncorrelated at different sites: $\langle \epsilon_n \epsilon_m \rangle = \delta_{nm}W^2/12$. This holds as well for the ground state field (20) in the high-density regime. However, the ground state correlation field ζ_ℓ has a finite range of correlations due to the presence of nearest-neighbor terms $G_{\ell\pm1}$ in its definition (6). As a consequence, the random potential $\varkappa_\ell$ is also correlated. Anderson localization with correlated disorder was studied in many publications (see Ref. [51] for continuum models and Refs. [52–55] for lattice models). The localization length of model (30) is calculated following Sec. 5.2.1 of the review [56] (see Appendix D for details):

$$\xi = \frac{96g^2a^2}{W^2}\frac{4 - E}{E(2 - E)^2}. \quad (32)$$

In the vicinity of $E = \lambda^2/(2gaJ) = 0$, we reobtain the known localization length divergence $\xi \simeq \frac{192g^3a^3J}{W^2\lambda^2}$. Notably, we discover an additional divergence of the localization length at finite energy $E = 2$, i.e., $\lambda = \pm2\sqrt{gaJ}$, as

$$\xi \simeq \frac{24g^3a^3J}{W^2(2\sqrt{gaJ} \pm \lambda)^2}, \quad |\lambda \pm 2\sqrt{gaJ}| \ll 2\sqrt{gaJ}. \quad (33)$$

The above singularity is the explanation for the observed side peak. We plot (32) in Fig. 5 for $a = 100$ and find quantitative agreement with the localization length data from transfer matrix evaluations of the exact and approximate equations while using the approximate GS field dependence as induced by the disorder. In particular, the peak position for the large density approximation from Eq. (27) agrees very well with the singularity position. In accord with our derivations from above, we expect the singularity to develop from the numerically observed finite height peak in the limit of infinite large densities.

C. Generalizations

Let us generalize to any lattice dimension with some hopping network or generalized discrete Laplacian:

$$i\dot{\psi}_\ell = \epsilon_\ell\psi_\ell + g|\psi_\ell|^2\psi_\ell - \mathcal{D}(\psi_\ell). \quad (34)$$

The discrete Laplacian

$$\mathcal{D}(\psi_\ell) = \sum_m J(\ell - m)\psi_m. \quad (35)$$

We assume $J(m) \geqslant 0$ to ensure the non-negativity of the ground state field G_l. Note that the Hamiltonian (1) is obtained with the choice $J(m) = J(\delta_{m,1} + \delta_{m,-1})$. It follows from the definition (35) that

$$gG_\ell^2 = ga - \epsilon_\ell + \delta\hat{\zeta}_\ell \geqslant 0 \quad (36)$$

and

$$\hat{\zeta}_\ell = \frac{1}{G_\ell}\mathcal{D}(G_\ell). \quad (37)$$

Note that with this definition the field $\hat{\zeta}_l$ includes the strength of the hopping network, as opposed to previous notations.

The exact equations for S_ℓ and D_ℓ take the form

$$\lambda S_\ell = (\hat{\zeta}_\ell + 2gG_\ell^2)D_\ell - \mathcal{D}(D_\ell) \quad (38)$$

$$\lambda D_\ell = \hat{\zeta}_\ell S_\ell - \mathcal{D}(S_\ell). \quad (39)$$

The approximate expression for the field G_ℓ in the high-density case is still given by Eq. (20), with all corrections due to the change in the hopping network and even the dimensionality appearing in higher-order corrections.

Since both $\hat{\zeta} \sim J$ and $\mathcal{D} \sim J$, we arrive at the generalized high-density BdG equations similar to the above-considered one-dimensional case with nearest-neighbor hopping as

$$\lambda^2 S_\ell = 2gG_\ell^2(\hat{\zeta}_\ell S_\ell - \mathcal{D}(S_\ell)). \quad (40)$$

Equations (20), (35), (37), and (40) constitute the generalization of the BdG equations in the high-density limit to any lattice dimension and hopping network. It remains to be studied whether these equations also result in a strong

enhancement of transport properties of disordered BdG modes at certain finite energies and momenta due to ground state correlations. An analysis of Eq. (40) for various 2D networks would be of interest in order to compare to the study of the Bose glass-superfluid quantum phase transitions in 2D disordered superconductors, which are controlled by the spatial localization of its excitations [42]. It remains an open question as to whether (40) admits any similar delocalization tendencies at finite energies in two-dimensional systems as found here for one-dimensional systems, and whether any delocalized phase can develop out of the mechanism studied here in one-dimensional systems.

V. CONCLUSION

We have studied in detail the properties of the ground state and small amplitude BdG excitations of the one-dimensional Gross-Pitaevskii lattice model in the presence of spatial disorder. On the numerical side, we computed the ground state energy density h as a function of the norm (particle) density a throughout the low- and high-density regimes. We applied perturbation approaches to both regimes and obtained analytical approximations of $h(a)$, the chemical potential, and the participation number density of the ground state, which characterizes its spatial distribution properties. The obtained analytical results agree quantitatively with full numerical computations.

We then proceeded to numerically compute the localization properties of small amplitude excitations above the ground state, which are coined Bogoliubov–de Gennes modes. We observe a divergence of their localization length for zero energy in full accord with previous publications. However, we also find an anomalous enhancement of the localization length of excitations in a side peak for finite energies in the high-density regime. We perform a systematic perturbation approach, which results in approximate eigenvalue equations, which are valid in the high-density regime. That eigenvalue problem corresponds to a one-dimensional tight-binding chain with nearest-neighbor hopping and correlated on-site disorder. We derive analytical expressions for the localization length as a function of energy. We then finally obtain a singularity and length divergence at a finite energy, which precisely corresponds to the numerically observed side peak. Therefore we conclude that a weakly excited disordered condensate in the regime of high density will allow for almost ballistic transport of excitations for selective finite energies and momenta. We also generalize the high-density equations for Bogoliubov–de Gennes modes for more complicated and higher-dimensional networks.

APPENDIX A: NUMERICAL DETAILS ON THE GROUND STATE CALCULATION

The wave-function amplitude is defined as $\psi_\ell = \sqrt{a_\ell}e^{i\phi_\ell}$, where a_ℓ is the local norm density, and ϕ_ℓ is the phase of the complex order parameter at each site with $0 \leqslant \phi_\ell \leqslant 2\pi$. It follows from Eq. (1) that the ground state is characterized by a vanishing phase difference between neighboring sites, $\phi_\ell = \phi$, and all the phases evolve in time keeping their phase difference zero [Eq. (5)]. Without loss of generality, we set $t = 0$ when all phases are equal to zero and define G_ℓ as a real variable.

Fixing the disorder realization and the desired average norm density a, we start iterating with a real random initial guess for G_ℓ in order to minimize the real function of H. The iteration is performed on five neighboring sites at a time using a function minimization algorithm [57], along with the normalization of G_ℓ according to $\sum_\ell G_\ell^2 = Na$. We shift the window of minimization by one site until all sites of the system are iterated once. We repeat this procedure 10–40 times until full convergence to the minimum energy is reached with a tolerance $< 10^{-15}$. We then test the numerical ground state G_ℓ such that the standard deviation of μ for each site found by Eq. (6) is much smaller than its mean for each realization of a system size N.

APPENDIX B: GROUND STATE AVERAGING FOR HIGH DENSITIES

For $a \geqslant W/2g$, we can define the average interaction of the neighboring sites as

$$\langle G_\ell G_{\ell+1} \rangle = \left\langle \sqrt{\left(a - \frac{\epsilon_\ell}{g}\right)\left(a - \frac{\epsilon_{\ell+1}}{g}\right)} \right\rangle. \quad \text{(B1)}$$

Different sites are uncorrelated, i.e., for arbitrary $f(x)$: $\langle f(\epsilon_i)f(\epsilon_j) \rangle = \langle f(\epsilon_i) \rangle \langle f(\epsilon_j) \rangle$, for $i \neq j$. Then

$$\frac{1}{N}\sum_i \langle f(\epsilon_i)f(\epsilon_j) \rangle = \left(\int d\epsilon\, \rho(\epsilon) f(\epsilon)\right)^2. \quad \text{(B2)}$$

By employing $f(\epsilon) = \sqrt{a - \epsilon/g}$ in Eq. (B2), we get

$$\left\langle \sqrt{\left(a - \frac{\epsilon_\ell}{g}\right)\left(a - \frac{\epsilon_{\ell+1}}{g}\right)} \right\rangle$$
$$= \left[\frac{1}{W}\int_{-\frac{W}{2}}^{\frac{W}{2}} d\epsilon \sqrt{a - \frac{\epsilon}{g}}\right]^2$$
$$= \left\{\frac{2}{3w}\left[\left(a + \frac{w}{2}\right)^{3/2} - \left(a - \frac{w}{2}\right)^{3/2}\right]\right\}^2, \quad \text{(B3)}$$

where $w = W/g$.

APPENDIX C: LOCALIZATION LENGTH: TRANSFER MATRIX METHOD

We solve Eq. (27) with the approximate GS field (20) with the transfer matrix method:

$$
\begin{bmatrix} S_{\ell+2} \\ S_{\ell+1} \\ S_\ell \\ S_{\ell-1} \end{bmatrix} = T_\ell \begin{bmatrix} S_{\ell+1} \\ S_\ell \\ S_{\ell-1} \\ S_{\ell-2}, \end{bmatrix},
\tag{C1}
$$

where the transfer matrix

$$
T_\ell = \begin{bmatrix} u_\ell + \zeta_{\ell+1} & \lambda^2/J^2 - 2 - u\zeta_\ell & u_\ell + \zeta_{\ell-1} & -1 \\ 1 & 0 & 0 & 0 \\ 0 & 1 & 0 & 0 \\ 0 & 0 & 1 & 0 \end{bmatrix},
\tag{C2}
$$

where $u_\ell = 2gG_\ell^2/J + \zeta_\ell$. Following Ref. [58], we start the transfer matrix multiplication with

$$
Q_0 = \begin{bmatrix} 1 & 0 \\ 0 & 1 \\ 0 & 0 \\ 0 & 0 \end{bmatrix}
\tag{C3}
$$

matrix with orthogonal columns, and multiply it by the transfer matrices $T_1 T_2 \dots T_N$. To control the round-off error, after each $q = 5$ iterations (number of multiplications by the transfer matrix $\hat{T}$), we apply QR decomposition, which gives two vectors: a normalized 2×4 matrix Q_j, and a 2×2 upper triangular matrix R_j:

$$
Q_j R_j = T_{(j-1)q+1} \dots T_{jq} Q_{j-1} \quad (j = 1, \dots, N/q).
\tag{C4}
$$

The smallest positive Lyapunov exponent can be estimated by

$$
\tilde{\gamma}_2 = \frac{1}{N} \sum_{j=1}^{N/q} \ln R_j(2, 2)
\tag{C5}
$$

in the limit $N \to \infty$. Here, in each QR factorization step, we store the second diagonal element of R_j, which has the smaller positive Lyapunov exponent. Practically, we need to use large but finite number of iterations: $N = 10^8$

$$
\xi = 1/\gamma_2.
\tag{C6}
$$

In addition, Eq. (29) can be solved by transfer matrix method:

$$
\begin{bmatrix} S_{\ell+1} \\ S_\ell \end{bmatrix} = T_\ell \begin{bmatrix} S_\ell \\ S_{\ell-1} \end{bmatrix},
\tag{C7}
$$

where

$$
T_\ell = \begin{bmatrix} \zeta_\ell - \lambda^2/2JgG_\ell^2 & -1 \\ 1 & 0 \end{bmatrix}.
\tag{C8}
$$

We start the transfer matrix multiplication with

$$
V_0 = \begin{bmatrix} 1 \\ 0 \end{bmatrix}
\tag{C9}
$$

vector, and multiply it by the transfer matrices: $V_j = T_j V_{j-1}$ $(j = 1, \dots, N)$. To deal with the round-off error,

after every five iterations, we normalize the vector V_j and estimate the smallest positive Lyapunov exponent by

$$
\tilde{\gamma}_1 = \frac{1}{N} \sum_{j=1}^{N/q} \ln \|V_j\|.
\tag{C10}
$$

After $N = 10^8$ iterations, we find the localization length ξ as

$$
\xi = 1/\tilde{\gamma}_1.
\tag{C11}
$$

APPENDIX D: LOCALIZATION LENGTH CALCULATION DETAILS IN THE HIGH-DENSITY REGIME

In this Appendix, we outline the computation of the localization length in the high-density regime as given by Eq. (32). We start from Eqs. (30), (31). In leading order $1/(ga)$ we obtain $\tilde{E} = 2 - E$ and the on-site disorder potential

$$
\varkappa_\ell = \frac{\epsilon_\ell(2 - 2E) - \epsilon_{\ell-1} - \epsilon_{\ell+1}}{2ga}.
\tag{D1}
$$

We define the on-site disorder correlation function

$$
K(n - m) = K(m - n) = \langle \varkappa_n \varkappa_m \rangle.
\tag{D2}
$$

The range of the correlations is finite because $K(\ell)$ takes nonzero values only for $\ell = 0, \pm1, \pm2$:

$$
K(0) = \langle \varkappa_\ell^2 \rangle = \frac{W^2}{48g^2a^2} \big((2 - 2E)^2 + 2\big),
\tag{D3}
$$

$$
K(1) = \langle \varkappa_\ell \varkappa_{\ell+1} \rangle = \frac{W^2}{24g^2a^2}(2E - 2),
\tag{D4}
$$

$$
K(2) = \langle \varkappa_\ell \varkappa_{\ell+2} \rangle = \frac{W^2}{48g^2a^2}.
\tag{D5}
$$

The Fourier transformed correlation function is then readily obtained:

$$
\begin{aligned}
K(q) &= \sum_\ell K(\ell) e^{iq\ell} \\
&= K(0) + 2 \sum_{\ell=1}^\infty K(\ell) \cos q\ell \\
&= \frac{W^2}{12g^2a^2} \Big((1 - E)^2 + \frac{1}{2} - 2(1 - E) \cos q \\
&\quad + \frac{1}{2} \cos 2q \Big).
\end{aligned}
\tag{D6}
$$

Next we compute the above expression at double argument value $K(2q)$ and then use the dispersion relationship of the homogeneous Eq. (30)

$$
E = 2[1 - \cos(q)]
\tag{D7}
$$

to replace q by E. After some additional simple algebra, the result reads

$$
K(2q) = \frac{W^2}{48g^2a^2} E^2(2 - E)^2.
\tag{D8}
$$

Anderson localization with correlated disorder was studied in many publications (see Ref. [51] for continuum models and Refs. [52–55] for lattice models). The inverse correlation

length in the model (30) is given by (see Sec. 5.2.1 of the review [56])

$$\frac{1}{\xi} = \frac{K(2q)}{8 \sin^2 q}. \tag{D9}$$

Substituting $K(2q)$ from (D8) into Eq. (D9) and using Eq. (D7) yield

$$\xi = \frac{96 g^2 a^2}{W^2} \frac{4 - E}{E(2 - E)^2}. \tag{D10}$$

[1] L. Pitaevskii and S. Stringari, *Bose-Einstein Condensation and Superfluidity* (Oxford University Press, Oxford, 2016).

[2] C. J. Pethick and H. Smith, *Bose-Einstein Condensation in Dilute Gases*, 2nd ed. (Cambridge University Press, Cambridge, 2008).

[3] F. Dalfovo, S. Giorgini, L. P. Pitaevskii, and S. Stringari, Theory of Bose-Einstein condensation in trapped gases, Rev. Mod. Phys. **71**, 463 (1999).

[4] A. J. Leggett, Superfluidity, Rev. Mod. Phys. **71**, S318 (1999).

[5] A. L. Fetter and A. A. Svidzinsky, Vortices in a trapped dilute Bose–Einstein condensate, J. Phys.: Condens. Matter **13**, R135 (2001).

[6] D. Jaksch, C. Bruder, J. I. Cirac, C. W. Gardiner, and P. Zoller, Cold Bosonic Atoms in Optical Lattices, Phys. Rev. Lett. **81**, 3108 (1998).

[7] J. Billy, V. Josse, Z. Zuo, A. Bernard, B. Hambrecht, P. Lugan, D. Clément, L. Sanchez-Palencia, P. Bouyer, and A. Aspect, Direct observation of Anderson localization of matter waves in a controlled disorder., Nature (London) **453**, 891 (2008).

[8] G. Roati, C. D'Errico, L. Fallani, M. Fattori, C. Fort, M. Zaccanti, G. Modugno, M. Modugno, and M. Inguscio, Anderson localization of a non-interacting Bose-Einstein condensate, Nature (London) **453**, 895 (2008).

[9] B. Deissler, M. Zaccanti, G. Roati, C. D.'Errico, M. Fattori, M. Modugno, G. Modugno, and M. Inguscio, Delocalization of a disordered bosonic system by repulsive interactions, Nat. Phys. **6**, 354 (2010).

[10] E. P. Gross, Structure of a quantized vortex in Boson systems, Il Nuovo Cimento **20**, 454 (1961).

[11] L. P. Pitaevskii, Vortex lines in an imperfect Bose gas, Sov. Phys. JETP. **13**, 451 (1961).

[12] K. O. Rasmussen, T. Cretegny, P. G. Kevrekidis, and N. Grønbech-Jensen, Statistical Mechanics of a Discrete Nonlinear System, Phys. Rev. Lett. **84**, 3740 (2000).

[13] A. Polkovnikov, S. Sachdev, and S. M. Girvin, Nonequilibrium Gross-Pitaevskii dynamics of boson lattice models, Phys. Rev. A **66**, 053607 (2002).

[14] T. Mithun, Y. Kati, C. Danieli, and S. Flach, Weakly Nonergodic Dynamics in the Gross-Pitaevskii Lattice, Phys. Rev. Lett. **120**, 184101 (2018).

[15] S. Iubini, L. Chirondojan, G.-L. Oppo, A. Politi, and P. Politi, Dynamical Freezing of Relaxation to Equilibrium, Phys. Rev. Lett. **122**, 084102 (2019).

[16] N. N. Bogoliubov, On the theory of superfluidity, J. Phys. USSR **11**, 23 (1947).

[17] N. N. Bogoliubov, The compensation principle and the self-consistent field method, Sov. Phys. Usp. **2**, 236 (1959).

[18] P.-G. De Gennes, *Superconductivity of Metals and Alloys* (CRC Press, Boca Raton, 2018).

[19] A. L. Fetter, Nonuniform states of an imperfect Bose gas, Ann. Phys. (NY) **70**, 67 (1972).

[20] P. W. Anderson, Absence of diffusion in certain random lattices, Phys. Rev. **109**, 1492 (1958).

[21] P. Lugan, D. Clement, P. Bouyer, A. Aspect, M. Lewenstein, and L. Sanchez-Palencia, Ultracold Bose Gases in 1D Disorder: From Lifshits Glass to Bose-Einstein Condensate, Phys. Rev. Lett. **98**, 170403 (2007).

[22] R. T. Scalettar, G. G. Batrouni, and G. T. Zimanyi, Localization in Interacting, Disordered, Bose Systems, Phys. Rev. Lett. **66**, 3144 (1991).

[23] P. Lugan, D. Clement, P. Bouyer, A. Aspect, and L. Sanchez-Palencia, Anderson Localization of Bogolyubov Quasiparticles in Interacting Bose-Einstein Condensates, Phys. Rev. Lett. **99**, 180402 (2007).

[24] Y. Kati, X. Yu, and S. Flach, Density resolved wave packet spreading in disordered Gross-Pitaevskii lattices, SciPost Phys. Core **3**, 6 (2020).

[25] X. Deng, R. Citro, A. Minguzzi, and E. Orignac, Phase diagram and momentum distribution of an interacting Bose gas in a bichromatic lattice, Phys. Rev. A **78**, 013625 (2008).

[26] L. Sanchez-Palencia and M. Lewenstein, Disordered quantum gases under control, Nat. Phys. **6**, 87 (2010).

[27] G. Modugno, Anderson localization in Bose–Einstein condensates, Rep. Prog. Phys. **73**, 102401 (2010).

[28] B. Shapiro, Cold atoms in the presence of disorder, J. Phys. A: Math. Theor. **45**, 143001 (2012).

[29] V. Gurarie, G. Refael, and J. T. Chalker, Excitations of One-Dimensional Bose-Einstein Condensates in a Random Potential, Phys. Rev. Lett. **101**, 170407 (2008).

[30] N. Bilas and N. Pavloff, Anderson localization of elementary excitations in a one-dimensional Bose-Einstein condensate, Eur. Phys. J. D **40**, 387 (2006).

[31] L. Fontanesi, M. Wouters, and V. Savona, Mean-field phase diagram of the one-dimensional Bose gas in a disorder potential, Phys. Rev. A **81**, 053603 (2010).

[32] T. A. L. Ziman, Localization and Spectral Singularities in Random Chains, Phys. Rev. Lett. **49**, 337 (1982).

[33] I. Avgin and D. Huber, Effect of quasiparticle renormalization on the localization of the excitations of a one-dimensional Bose–Einstein condensate in a random potential, Phys. B: Condens. Matter **406**, 1906 (2011).

[34] M. Kramer, C. Menotti, L. Pitaevskii, and S. Stringari, Bose-Einstein condensates in 1D optical lattices, Eur. Phys. J. D **27**, 247 (2003).

[35] C. Gaul and C. A. Müller, Bogoliubov excitations of disordered Bose-Einstein condensates, Phys. Rev. A **83**, 063629 (2011).

[36] C. Gaul and C. A. Müller, Bogoliubov theory on the disordered lattice, Eur. Phys. J.: Spec. Top. **217**, 69 (2013).

[37] C. Gaul, P. Lugan, and C. A. Müller, Anderson localization of bogoliubov excitations on quasi–1D strips, Ann. Phys. (NY) **527**, 531 (2015).

[38] M. P. A. Fisher, P. B. Weichman, G. Grinstein, and D. S. Fisher, Boson localization and the superfluid-insulator transition, Phys. Rev. B **40**, 546 (1989).

[39] W. Krauth, N. Trivedi, and D. Ceperley, Superfluid-Insulator Transition in Disordered Boson Systems, Phys. Rev. Lett. **67**, 2307 (1991).

[40] M. Feigelman, V. Geshkenbein, L. Ioffe, and A. Larkin, Two-dimensional Bose liquid with strong gauge-field interaction, Phys. Rev. B **48**, 16641 (1993).

[41] G. Seibold, L. Benfatto, C. Castellani, and J. Lorenzana, Superfluid Density and Phase Relaxation in Superconductors with Strong Disorder, Phys. Rev. Lett. **108**, 207004 (2012).

[42] J. P. Á. Zúñiga and N. Laflorencie, Bose-Glass Transition and Spin-Wave Localization for 2D Bosons in a Random Potential, Phys. Rev. Lett. **111**, 160403 (2013).

[43] J. P. Álvarez Zúniga, D. J. Luitz, G. Lemarié, and N. Laflorencie, Critical Properties of the Superfluid-Bose-Glass Transition in Two Dimensions, Phys. Rev. Lett. **114**, 155301 (2015).

[44] E. V. Doggen, G. Lemarié, S. Capponi, and N. Laflorencie, Weak-versus strong-disorder superfluid-Bose glass transition in one dimension, Phys. Rev. B **96**, 180202(R) (2017).

[45] B. Sacépé, T. Dubouchet, C. Chapelier, M. Sanquer, M. Ovadia, D. Shahar, M. Feigel'Man, and L. Ioffe, Localization of preformed cooper pairs in disordered superconductors, Nat. Phys. **7**, 239 (2011).

[46] A. Kamlapure, T. Das, S. C. Ganguli, J. B. Parmar, S. Bhattacharyya, and P. Raychaudhuri, Emergence of nanoscale inhomogeneity in the superconducting state of a homogeneously disordered conventional superconductor, Sci. Rep. **3**, 1 (2013).

[47] G. Blatter, M. V. Feigel'man, V. B. Geshkenbein, A. I. Larkin, and V. M. Vinokur, Vortices in high-temperature superconductors, Rev. Mod. Phys. **66**, 1125 (1994).

[48] C. Rubio-Verdu, A. M. Garcia-garcia, H. Ryu, D.-J. Choi, J. Zaldivar, S. Tang, B. Fan, Z.-X. Shen, S.-K. Mo, and J. I. Pascual, Visualization of multifractal superconductivity in a two-dimensional transition metal dichalcogenide in the weak-disorder regime, Nano Lett. **20**, 5111 (2020).

[49] B. Kramer and A. MacKinnon, Localization: theory and experiment, Rep. Prog. Phys. **56**, 1469 (1993).

[50] K. Ishii, Localization of eigenstates and transport phenomena in the one-dimensional disordered system, Prog. Theor. Phys. Suppl. **53**, 77 (1973).

[51] I. M. Lifshits, S. A. Gredeskul, and L. Pastur, *Introduction to the Theory of Disordered Systems* (Wiley, New York, 1988).

[52] M. Griniasty and S. Fishman, Localization by Pseudorandom Potentials in One Dimension, Phys. Rev. Lett. **60**, 1334 (1988).

[53] J. M. Luck, Cantor spectra and scaling of gap widths in deterministic aperiodic systems, Phys. Rev. B **39**, 5834 (1989).

[54] F. M. Izrailev and A. A. Krokhin, Localization and the Mobility Edge in One-Dimensional Potentials with Correlated Disorder, Phys. Rev. Lett. **82**, 4062 (1999).

[55] M. Titov and H. Schomerus, Nonuniversality of Anderson Localization in Short-Range Correlated Disorder, Phys. Rev. Lett. **95**, 126602 (2005).

[56] F. Izrailev, A. Krokhin, and N. Makarov, Anomalous localization in low-dimensional systems with correlated disorder, Phys. Rep. **512**, 125 (2012).

[57] J. C. Lagarias, J. A. Reeds, M. H. Wright, and P. E. Wright, Convergence Properties of the Nelder-Mead Simplex Method in Low Dimensions, SIAM J. Opt. **9**, 112 (1998).

[58] K. Slevin and T. Ohtsuki, Critical exponent for the anderson transition in the three-dimensional orthogonal universality class, New J. Phys. **16**, 015012 (2014).